Ultrasound Obstet Gynecol 2021; **58**: 254–263
Published online 6 July 2021 in Wiley Online Library (wileyonlinelibrary.com). **DOI:** 10.1002/uog.22162.

Normal human brainstem development *in vivo*: a quantitative fetal MRI study

G. O. DOVJAK[1], V. SCHMIDBAUER[1], P. C. BRUGGER[2], G. M. GRUBER[3], M. DIOGO[1], S. GLATTER[1], M. WEBER[1], B. ULM[4], D. PRAYER[1] and G. J. KASPRIAN[1]

[1]*Department of Biomedical Imaging and Image-Guided Therapy, Medical University of Vienna, Vienna, Austria;* [2]*Center for Anatomy and Cell Biology, Department of Anatomy, Medical University of Vienna, Vienna, Austria;* [3]*Department of Anatomy and Biomechanics, Karl Landsteiner University of Health Sciences, Krems, Austria;* [4]*Department of Obstetrics and Feto-Maternal Medicine, Medical University of Vienna, Vienna, Austria*

KEYWORDS: brainstem; brainstem planimetry; fetal MRI; hindbrain malformation; Magnetic resonance imaging; MRI; neurodevelopment; posterior fossa

CONTRIBUTION

What are the novel findings of this work?
The substructures of the fetal brainstem follow a distinct spatiotemporal growth pattern during the second and third trimesters of pregnancy. This is characterized by a significant change in their relative cross-sectional areal contributions, measured in the midsagittal plane using fetal magnetic resonance imaging, with an increase in the area of the pons and a decrease in that of the midbrain relative to the total brainstem area. Reference data for diameters and areas of the brainstem and cerebellum are provided from 15 to 40 gestational weeks.

What are the clinical implications of this work?
Caution is needed when interpreting fetal brainstem appearance during the early second trimester, as these brainstem proportions differ significantly from the adult morphology. With the provided reference data, fetal brainstem morphology can be quantified.

ABSTRACT

Objectives *To characterize spatiotemporal growth differences of prenatal brainstem substructures and cerebellum, using linear biometry and planimetry on fetal magnetic resonance imaging (MRI).*

Methods *In this retrospective study, we included fetuses with normal brain and a precise midsagittal T2-weighted brain MRI sequence obtained between May 2003 and April 2019. The cross-sectional area, rostrocaudal diameter and anteroposterior diameter of the midbrain, pons (basis pontis and pontine tegmentum), medulla oblongata and cerebellar vermis, as well as the transverse cerebellar diameter, were quantified by a single observer. The diameters were also assessed by a second observer to test inter-rater variability.*

Results *We included 161 fetuses with normal brain and a precise midsagittal MRI sequence, examined at a mean ± SD gestational age of 25.7 ± 5.4 (range, 14 + 0 to 39 + 2) weeks. All substructures of the fetal brainstem and the cerebellum could be measured consistently (mean ± SD interobserver intraclass correlation coefficient, 0.933 ± 0.065). We provide reference data for diameters and areas of the brainstem and cerebellum in the second and third trimesters. There was a significant quadratic relationship between vermian area and gestational age, and all other measured parameters showed a significant linear growth pattern within the observed period (*$P < 0.001$*). A significant change in the relative proportions of the brainstem substructures occurred between the beginning of the second trimester and the end of the third trimester, with an increase in the area of the pons (*$P < 0.001$*) and a decrease in that of the midbrain (*$P < 0.001$*), relative to the total brainstem area.*

Conclusions *The substructures of the fetal brainstem follow a distinct spatiotemporal growth pattern, characterized by a relative increase in the pons and decrease in the midbrain, between 15 and 40 weeks of gestation.*

Correspondence to: Prof. G. J. Kasprian, Department of Biomedical Imaging and Image-Guided Therapy, Medical University of Vienna, Waehringer Guertel 18-20, 1090 Vienna, Austria (e-mail: Gregor.Kasprian@meduniwien.ac.at)

Accepted: 10 July 2020

Caution is needed when interpreting fetal brainstem appearance during the early second trimester, as the brainstem proportions differ significantly from the adult morphology. The reference data provided herein should help to increase diagnostic accuracy in detecting disorders of defective hindbrain segmentation.

INTRODUCTION

The brainstem controls several critical functions, including respiration, arousal and sleep and blood pressure, as well as controlling eye movements, and is composed of numerous complex nuclei and connecting pathways. Prenatal characterization of brainstem pathology with ultrasound and magnetic resonance imaging (MRI) is considered difficult. Due to its small dimensions, the identification of subtle alterations in the brainstem requires an extensive background in fetal neurosonography and fetal MRI. Moreover, the morphology of the fetal brainstem and cerebellum undergo distinct changes during gestation, characterized by a pronounced increase in volume and proportional changes, which are not, as yet, widely appreciated[1]. From pediatric and adult MRI, it is known that the normal ratio of the rostrocaudal diameters of the midbrain, pons and medulla oblongata is about 1:2:1[2].

Posterior fossa biometry is valuable in diagnostic decision-making and can alter the prediction of potential risk with regard to a poor neurological outcome[3]. Even changes in simple measurements, such as a reduction in the transverse cerebellar diameter, may serve as a predictor of further anomalies[4]. Sonographic studies have been published that report nomograms of normal posterior fossa structures and their application in different midbrain-hindbrain diseases[5–9]. Similarly, multiple biometric fetal MRI studies have been reported, usually focusing on the period between 20 gestational weeks and the end of pregnancy[10–17]. These studies provide various measurements of brainstem structures (mainly the anteroposterior (AP) diameter of the pons), but focus primarily on the cerebellum (rostrocaudal, AP and transcerebellar diameter). The areas of brainstem substructures have not yet been assessed.

In this retrospective MRI study, we aimed to integrate common posterior fossa measurements, such as the rostrocaudal and AP diameters of the fetal midbrain, pons, medulla oblongata and cerebellar vermis, as well as the transverse cerebellar diameter, with area/planimetric measurements of the fetal brainstem substructures. In so doing, we hoped to elucidate whether the spatial dimensions and the relative contribution of the different brainstem subdivisions in the fetus are comparable to those in the adult. These biometric data are presented as reference charts with percentiles from the early second trimester to term.

METHODS

Subjects

In this retrospective fetal MRI study, all examinations were performed and evaluated at the Department of Biomedical Imaging and Image-guided Therapy of the Medical University of Vienna. Potential subjects with normal brain development, as assessed by prenatal ultrasound and fetal MRI, and a precise midsagittal slice on T2-weighted MRI, obtained between May 2003 and April 2019, were identified retrospectively in the hospital's Picture Archiving and Communication System (PACS) database. The midsagittal plane was defined as depicting the fetal nose, corpus callosum, brainstem and cerebellar vermis in their entirety (Figure 1a). Sequences with marked motion artifacts or oblique planes, as well as multiple pregnancies, were excluded. All cases were clinically indicated and had been referred for fetal MRI after a standard neurosonographic examination by an obstetrician (Level-II or Level-III sonographer, according to European standards). The indications for MRI were primarily body malformations or premature rupture of the membranes. Cases with brain malformations, as well as those known to have genetic abnormalities or syndromes, were excluded, but there was no systematic genetic testing. All available fetuses who met these criteria were included; a sample-size analysis was not performed in this exploratory study. Gestational age was determined by biometry at the first sonographic examination and is presented as weeks post-menstruation. In our institution, it is standard practice to round up gestational age, such that, for example, $14+0$ to $14+6$ weeks is represented as 15 gestational weeks. This study was approved by the local institutional review board (ethics committee number 2175/2019). All mothers had given written, informed consent to undergo fetal MRI and agreed to the scientific use of their imaging data.

Magnetic resonance imaging

Examinations were performed using a 1.5-Tesla (T) scanner (Ingenia, Philips Healthcare, Endhoven, The Netherlands) or a 3-T scanner (Achieva, Philips Healthcare), in accordance with the fetal MRI guidelines of the International Society of Ultrasound in Obstetrics and Gynecology[18]. A body coil was used and precise, midsagittal T2-weighted turbo spin-echo sequences with the following specifications were acquired: in-plane resolution, 0.62/0.62–1.17/1.17 mm; slice thickness, 2.0–4.5 mm; matrix size, 256×256; field of view, 200–230 mm; relaxation time, $\leq 20\,000$ ms; echo time, 100–140 ms. The image data were exported and all measurements for the purposes of this study were performed using the open-source software application, ITK Snap, version 3.8[19]. The diameters of brainstem structures in all fetuses were measured independently by two observers (G.D., V.S.), both of whom had at least 2 years' experience of fetal MRI. Planimetry of brainstem substructures and the cerebellar vermis was performed together by both observers.

In all examined fetuses, the brainstem and vermian diameters (Figure 1b) were quantified according to the following anatomical reference landmarks. The midbrain rostrocaudal diameter was measured parallel to the tectum, between its superior and inferior borders, and the AP diameter was measured perpendicular to this line. The rostrocaudal diameter of the pons was measured from the level of the pontomesencephalic junction to the pontomedullary junction, parallel to the posterior border of the pons. The AP diameter at the mid-level of the pons was differentiated into the diameter of the basis pontis and that of the pontine tegmentum, these being separated by a line from the superior to the inferior pontine notch. The rostrocaudal diameter of the medulla oblongata was measured similarly, parallel to the posterior border of the brainstem substructure, from the pontomedullary junction to the level of the obex, and the AP diameter was perpendicular to this line. The rostrocaudal diameter of the cerebellar vermis was measured parallel to the posterior border of the brainstem and the AP diameter was measured from the fastigial point to the most posterior vermian border. Corresponding to the diameters, the cross-sectional areas of the brainstem substructures and the vermis were measured (Figure 1c). The transverse cerebellar diameter was measured in the coronal plane (Figure 1d).

Statistical analysis

All analyses were carried out using IBM SPSS Statistics for Windows software (version 26; IBM Corp., Armonk, NY, USA) and statistics software R, version 3.6.3 (https://www.r-project.org). Due to heteroscedasticity (heterogeneous variances of residuals) and highly skewed residuals, and based on the selection standards of the World Health Organization for the methods by which to measure growth curves in children[20], a generalized additive model for location, scale and shape (GAMLSS) with a Box-Cox t distribution (R package 'gamlss') was used to calculate the percentile curves of all measured parameters[21].

The mean and SD gestational age at MRI (in weeks) was calculated. Pearson's correlation was assessed for each of the evaluated parameters with gestational age. *t*-tests were performed to compare the relative contribution to the brainstem area of the midbrain, pons and medulla oblongata between fetuses in the first

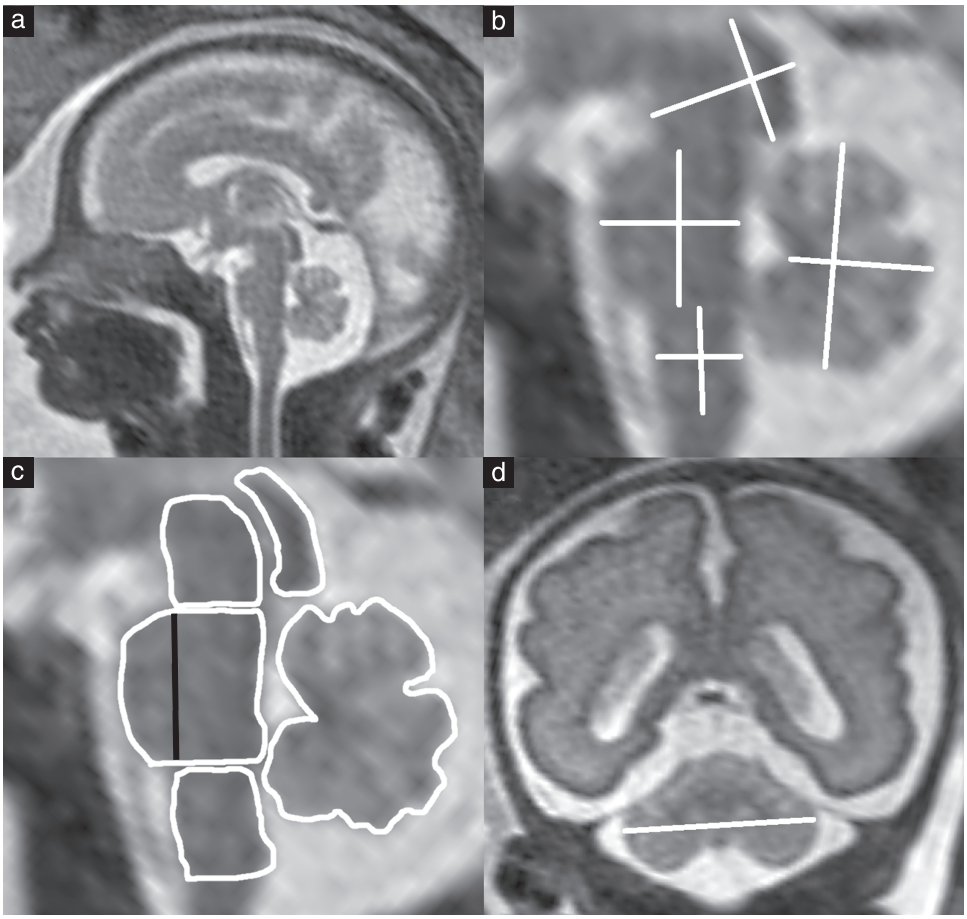

Figure 1 (a) T2-weighted midsagittal magnetic resonance image of fetal head at 28 + 4 weeks. Zoomed-in images showing measurement of diameters (b) and planimetry (c) of brainstem substructures (midbrain, pons, medulla oblongata) and the cerebellar vermis. The transverse cerebellar diameter was measured in the coronal plane (d). The areas and anteroposterior (AP) diameters of the basis pontis, pontine tegmentum and total pons were measured separately ((b) shows total pons AP diameter; (c) shows subdivision of the pons, indicated by the black line).

5 gestational weeks (weeks 15–19) evaluated and those in the last 5 weeks (weeks 36–40). We performed paired *t*-tests on age-matched cases to check for differences in measurements from sequences obtained using 1.5-T compared with 3-T MRI, and to compare measurements between the subgroup of fetuses with normal brain but pathological fetal or maternal findings and the subgroup with no pathological findings. $P \leq 0.05$ was considered statistically significant. To avoid an increasing type-2 error, no multiplicity corrections were performed. To test the inter-rater variability and reliability, we calculated the intraclass correlation coefficient (ICC) between the two observers for all diameters. ICC > 0.75 was considered to indicate excellent correlation[22].

RESULTS

After screening existing fetal MRI reports, 164 fetuses with normal brain were identified, of which three were excluded due to motion artifacts or an oblique midsagittal plane. Thus, our study group included 161 fetuses with normal brain and a precise midsagittal MRI sequence. The main indications for MRI were limb or body malformations (Table S1), and the indications in the youngest fetuses were all maternal. The mean ± SD gestational age at examination was 25.7 ± 5.4 (range, 14 + 0 to 39 + 2) weeks (Table S2). The mean ± SD gestational age of the group examined with a 1.5-T scanner ($n = 145$) was 25.9 ± 5.3 (range, 14 + 0 to 39 + 2) weeks and that in the 3-T group ($n = 16$) was 23.0 ± 5.9 (range, 16 + 0 to 37 + 0) weeks. In the group without any pathological findings were 23 fetuses, with a mean ± SD gestational age of 27.3 ± 5.1 (range, 17 + 4 to 38 + 2) weeks, and in the remaining group with normal brain but pathological fetal or maternal findings were 138 fetuses, with a mean ± SD gestational age of 25.4 ± 5.4 (range, 14 + 0 to 39 + 2) weeks.

There was excellent correlation of all diameter measurements between the two observers, with an overall mean ± SD ICC of 0.933 ± 0.065 (range, 0.804 (midbrain rostrocaudal diameter) to 0.996 (transcerebellar diameter)).

There was a significant quadratic relationship between vermian area and gestational age, and all other measured parameters showed a significant linear relationship with gestational age ($P < 0.001$). Pearson's correlation coefficients ranged from 0.654 (correlation of basis pontis AP diameter with pontine tegmentum AP diameter) to 0.977 (correlation of pons area to pontine tegmentum area). Table 1 presents the constants (k and d) required to solve the linear equation for the 5th, 25th, 50th, 75th and 95th percentiles (size in mm or mm^2 = (gestational age in weeks × k) + d) of each measured brain structure, with the exception of vermian area, whose percentiles are given in Table 2.

Figure 2 presents plots of the areas of evaluated brainstem substructures and cerebellar vermis in all fetuses. The 5th, 25th, 50th, 75th and 95th percentiles of each structure are marked for reference. The cerebellar vermis was the structure in the posterior fossa whose area increased most during the evaluated period of gestation, with a size at the end of pregnancy that was

Table 1 Values for calculation of percentiles (5th, 25th, 50th, 75th and 95th) for fetal brainstem substructural and cerebellar measurements, according to the linear equation: size (in mm or mm^2) = (gestational age in weeks × k) + d

	5th percentile		*25th percentile*		*50th percentile*		*75th percentile*		*95th percentile*	
Fetal brain measurement	*k*	*d*	*k*	*d*	*k*	*d*	*k*	*d*	*k*	*d*
Midbrain										
Area (in mm^2)	2.81	−14.26	3.11	−15.78	3.35	−16.99	3.62	−18.38	4.10	−20.81
RC diameter (in mm)	0.19	2.59	0.21	2.80	0.22	2.96	0.23	3.14	0.25	3.42
AP diameter (in mm)	0.31	1.96	0.34	2.11	0.35	2.21	0.37	2.32	0.40	2.47
Total pons										
Area (in mm^2)	5.05	−62.26	5.79	−71.34	6.28	−77.35	6.79	−83.71	7.70	−94.82
RC diameter (in mm)	0.39	−1.97	0.44	−2.22	0.48	−2.38	0.51	−2.55	0.55	−2.78
AP diameter (in mm)	0.33	−0.59	0.36	−0.64	0.38	−0.68	0.40	−0.72	0.44	−0.78
Basis pontis										
Area (in mm^2)	1.79	−23.89	2.14	−28.50	2.43	−32.42	2.81	−37.43	3.64	−48.51
AP diameter (in mm)	0.14	−0.91	0.17	−1.09	0.19	−1.22	0.21	−1.36	0.25	−1.57
Pontine tegmentum										
Area (in mm^2)	2.88	−33.02	3.37	−38.64	3.72	−42.59	4.07	−46.58	4.58	−52.39
AP diameter (in mm)	0.14	0.70	0.16	0.80	0.17	0.87	0.19	0.94	0.21	1.05
Medulla oblongata										
Area (in mm^2)	2.60	−22.60	3.01	−26.13	3.27	−28.44	3.55	−30.84	4.01	−34.83
RC diameter (in mm)	0.23	2.33	0.25	2.59	0.27	2.76	0.29	2.92	0.31	3.15
AP diameter (in mm)	0.19	0.34	0.21	0.38	0.23	0.41	0.25	0.45	0.28	0.49
Cerebellar vermis										
RC diameter (in mm)	0.72	−6.83	0.79	−7.48	0.84	−7.90	0.88	−8.32	0.95	−8.93
AP diameter (in mm)	0.53	−5.26	0.57	−5.69	0.60	−6.02	0.64	−6.38	0.70	−6.99
Transcerebellar diameter (in mm)	1.52	−12.48	1.60	−13.13	1.66	−13.60	1.72	−14.15	1.85	−15.23

AP, anteroposterior; RC, rostrocaudal.

22.5-fold larger than the size at 15 weeks. In comparison, the brainstem increased 5.6-fold overall, resulting in a pronounced shift in the brainstem–vermian ratio, from 5.3 to 1.3. The pons was the brainstem substructure with the greatest increase in area (10.1-fold), followed by the medulla oblongata (5.3-fold) and the midbrain (3.3-fold). The basis pontis increased 13.3-fold and the pontine tegmentum increased 8.5-fold. The contribution of the basis pontis to the total pons area increased moderately, from 33.3% in the early second trimester to 44.0% at the end of pregnancy. The areal contribution of the different brainstem substructures changed markedly during the time period examined, with the ratio of midbrain to pons to medulla oblongata ranging from 2:1:1 at 15 weeks' gestation, to 3:2:2 at 18 weeks, to 1:1:1 at 21 weeks, to 2:3:2 at the end of pregnancy. These changes were driven mainly by a relative increase in the areal contribution of the pons and a relative decrease in the areal contribution of the midbrain (Figure 3). The areal contribution to the brainstem of the pons (30.9%–44.1%) and the midbrain (41.2%–28.9%) each changed significantly ($P < 0.001$ for each) between the first 5 and the last 5 evaluated weeks of gestation, while the areal contribution of the medulla oblongata remained nearly the same, being 27.9% in the first 5 weeks of the study period and 27.0% in the last 5 weeks ($P = 0.332$).

Figure 4 presents plots of the three evaluated cerebellar parameters (vermian rostrocaudal and AP diameters, and transcerebellar diameter) and the diameters of all brainstem substructures. These showed linear growth, with the transverse cerebellar diameter having the least measurement spread. Similar to the area measurements, the largest increase (in both AP and rostrocaudal diameters) during the gestational time period examined was observed in the vermis, and the second largest was in the pons.

For the comparison of measurements in sequences obtained by a 1.5-T and a 3-T MRI scanner, 15 age-matched pairs could be formed. The differences in mean values between measurements performed in sequences obtained using the two different field strengths were small (mean ± SD difference for areas, $3.39 \pm 1.71\,mm^2$; for diameters, 0.21 ± 0.10 mm) and without significance, with the greatest difference in area being for the total pons ($5.78\,mm^2$) and the greatest difference in diameter being in the AP diameter of the pons (0.41 mm).

For the comparison between fetuses with no pathological findings and those with normal brain but other fetal or maternal pathological findings, 23 age-matched pairs were formed, among which we found no significant differences (mean ± SD difference for diameters, 0.21 ± 0.18 mm; for areas, $1.57 \pm 0.91\,mm^2$). The greatest difference in length was for the AP diameter of the vermis (0.61 mm) and the greatest difference in area was of the vermis ($3.11\,mm^2$).

Table 2 Cross-sectional area percentiles (5th, 25th, 50th, 75th and 95th) in mm^2 for fetal cerebellar vermis

Gestational week	*Percentile*				
	5th	*25th*	*50th*	*75th*	*95th*
15	9.499	10.975	11.806	12.669	14.374
16	14.519	16.774	18.045	19.364	21.971
17	20.150	23.279	25.042	26.873	30.491
18	26.390	30.489	32.798	35.195	39.934
19	33.241	38.403	41.312	44.332	50.301
20	40.701	47.023	50.585	54.282	61.590
21	48.772	56.347	60.615	65.046	73.803
22	57.453	66.376	71.404	76.623	86.940
23	66.745	77.111	82.951	89.014	100.999
24	76.646	88.550	95.257	102.219	115.982
25	87.157	100.694	108.321	116.238	131.888
26	98.279	113.543	122.143	131.070	148.717
27	110.011	127.096	136.723	146.716	166.470
28	122.353	141.355	152.062	163.176	185.146
29	135.305	156.319	168.159	180.449	204.745
30	148.867	171.987	185.014	198.537	225.267
31	163.039	188.360	202.627	217.437	246.713
32	177.821	205.439	220.999	237.152	269.082
33	193.214	223.222	240.129	257.680	292.374
34	209.217	241.710	260.018	279.022	316.590
35	225.830	260.903	280.664	301.178	341.729
36	243.053	280.801	302.069	324.148	367.791
37	260.886	301.404	324.233	347.931	394.776
38	279.329	322.711	347.154	372.528	422.685
39	298.382	344.724	370.834	397.938	451.517
40	318.046	367.441	395.272	424.163	481.272

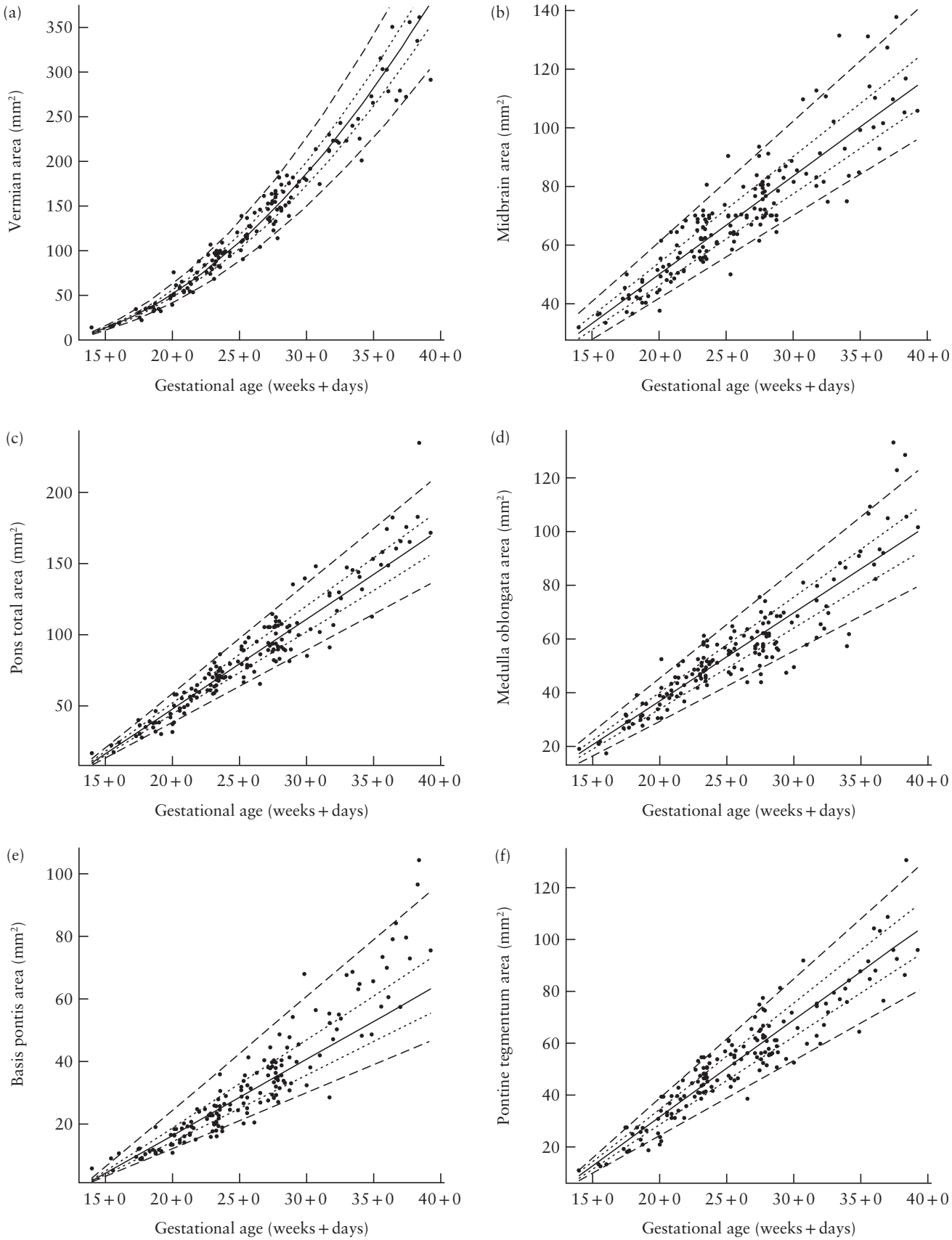

Figure 2 Scatterplots of areas of the brainstem substructures and cerebellar vermis in the normal fetal brain according to gestational age in weeks + days. Lines indicate 5th, 25th, 50th, 75th and 95th percentiles.

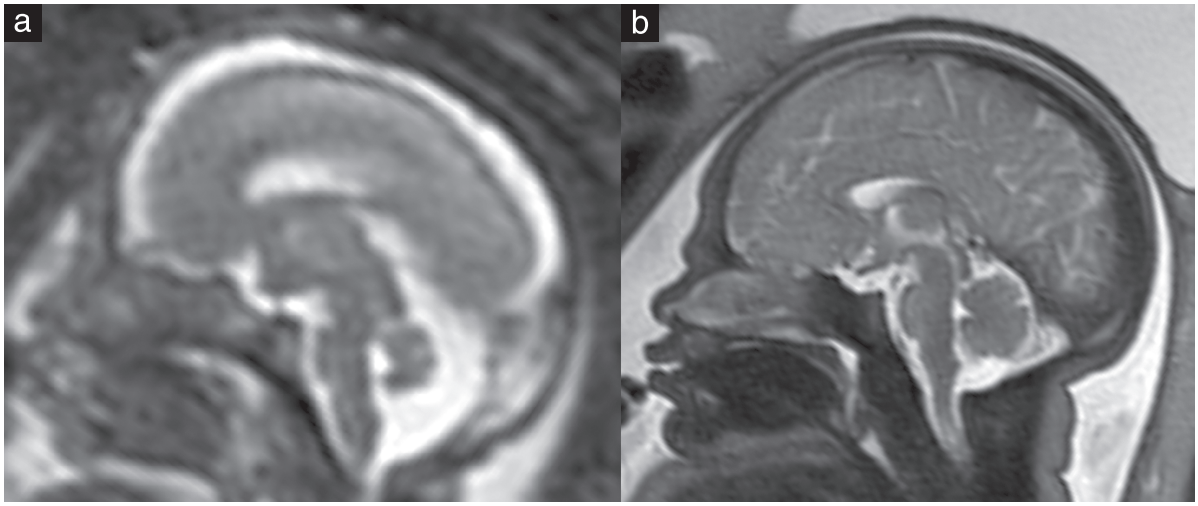

Figure 3 Comparison of the brain of an 18 + 5-week (a) and a 36 + 1-week (b) fetus on T2-weighted magnetic resonance imaging. In the younger fetus, the areal contribution of the midbrain is significantly greater than that of the pons (41.7% *vs* 33.9%), whereas, in the older fetus, this relationship is reversed (32.3% *vs* 43.6%).

DISCUSSION

In this retrospective fetal MRI study, we demonstrated that the fetal brainstem undergoes specific spatiotemporal changes, with a relative increase in area of the pons and decrease in that of the midbrain, during the second and third trimesters. During the development of the central nervous system, the future brainstem undergoes a segmentation process that leads to patterning along the AP and dorsoventral neuraxis[23]. After formation of the neural tube, the primary brain vesicles, the mesencephalon and rhombencephalon, develop into the brainstem and cerebellum. The midbrain originates from the mesencephalon, while the rhombencephalon diverges further into the secondary brain vesicles, the metencephalon (which gives rise to the cerebellum and rostral pons) and the myelencephalon (predecessor of the caudal pons and medulla oblongata)[24]. The precise positioning, area and diameters of brainstem subunits are defined by multiple genes and factors involved in the AP and dorsoventral patterning process, in which the isthmic organizer is crucial. This *FGF8*-expressing, constrictive formation is located between the expanding rostral mesencephalon and the caudal cerebellum and regulates spatial regionalization through diverse signaling pathways[25]. The molecular midbrain-hindbrain border is determined by *Otx2* expression rostrally and *Gbx2* expression caudally[26]. The cerebellum develops from the upper rhombic lip at the level of rhombomere 1[27,28]. Due to the complexity of the hindbrain patterning processes, many developmental pathologies become morphologically apparent through abnormal spatiotemporal patterning of the brainstem[29]. To increase diagnostic certainty in the detection of subtle pathologies prenatally, a thorough understanding of the changing appearance of the fetal brainstem and its quantitative aspects is required. Morphological analysis and pattern recognition on MRI of posterior fossa structures is more important in the fetal setting than in the postnatal setting, as some parents refuse invasive testing because of the small risk of pregnancy loss[30], and genetic testing is often not available. Even when it is, the yield of genetic testing in midbrain-hindbrain malformations varies. Some authors emphasize that the evaluation of brainstem patterning should play a central role in directing genetic screening[31]. Systematic brain biometry is an essential instrument with which to confirm or disprove the regular development of the fetus[12].

Not surprisingly, all diameters and areas evaluated in this study showed a significant and strong correlation with gestational age. This is in accordance with other biometric ultrasound and fetal MRI studies, which showed a linear relationship[6–8,14]. The areas of the cerebellar vermis and pons showed the greatest increase over the time period studied. This is neuroanatomically plausible, as these structures are connected via multiple fibers. The most prominent of these fibers are the main afferent cerebellar tracts that originate in the pontine nuclei, traversing from each side of the pons to the other, and enter the cerebellum via the middle cerebellar peduncle[32,33]. The increase in the size of the pons seems to be driven by growth of the basis pontis, which showed a relative increase, from 33% of the total pons area in the early second trimester to 44% at the end of pregnancy. This has also been demonstrated by anatomical studies and was suspected to be caused by a considerable increase in the numbers of cells in the pontine nuclei of the ventral pons, in addition to growth of the pontocerebellar axons[34]. We found that the areal ratio of brainstem substructures also reflected the pronounced pontine growth during gestation, with the midbrain to pons to medulla oblongata area ratio changing extensively during the second and third trimesters, from 2:1:1 in the early second trimester to 2:3:2 at the end of pregnancy.

There was no difference in our subgroup analysis comparing 1.5-T and 3-T MRI, and there was no difference in the age-matched comparison between fetuses

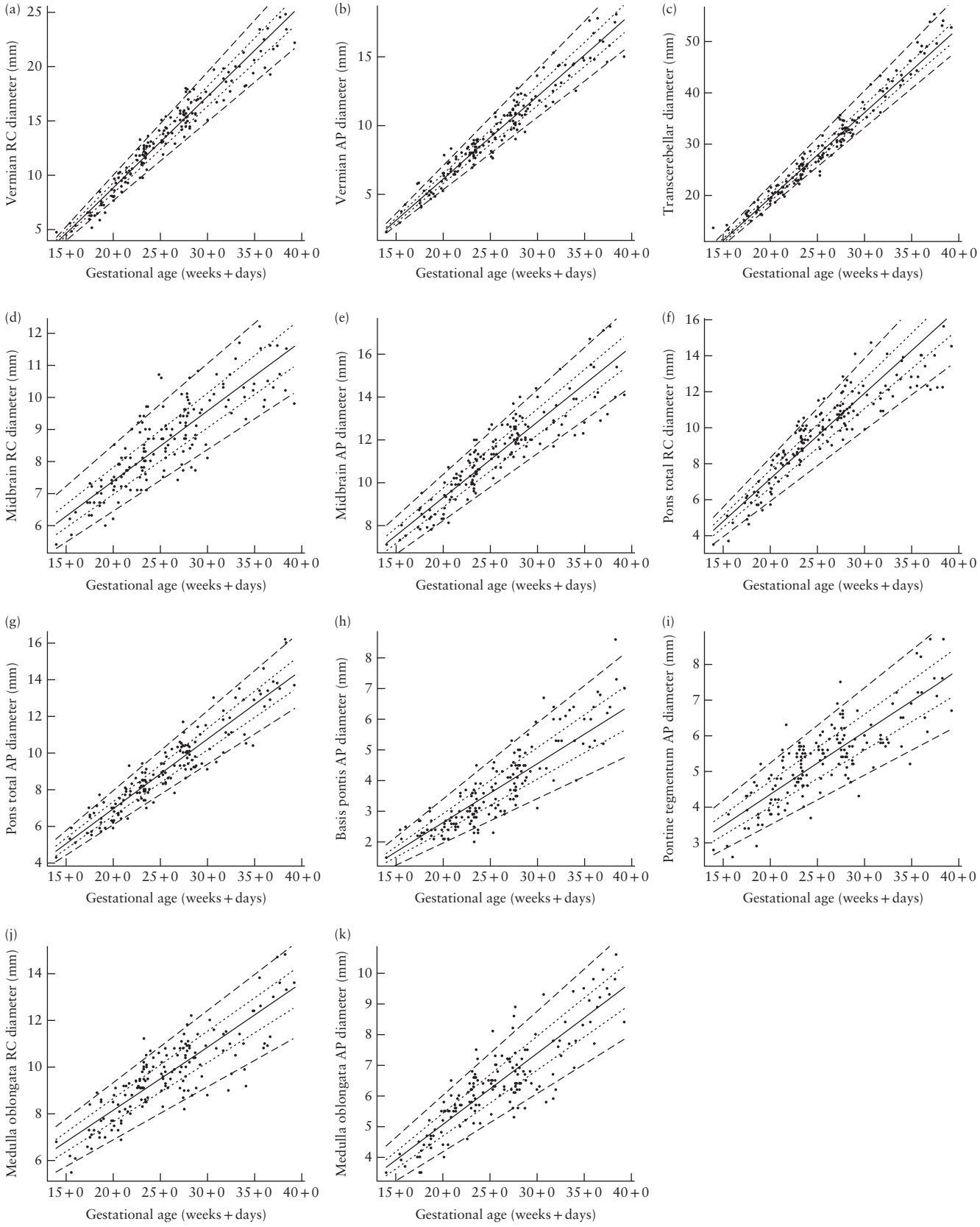

Figure 4 Scatterplots of rostrocaudal (RC) and anteroposterior (AP) diameters of the brainstem substructures and cerebellum in the normal fetal brain according to gestational age in weeks + days. Lines indicate 5th, 25th, 50th, 75th and 95th percentiles.

with no pathological findings and those with normal brain but other fetal or maternal pathological findings. The ICC showed excellent correlation between observers, with a mean value of 0.933, indicating that these measurements are reproducible and reliable in the assessment of fetal MRI biometry.

The biometric fetal MRI data presented in this study can be applied in a variety of midbrain-hindbrain malformations. Among these are genetic syndromes, such as the group of pontocerebellar hypoplasias, which were described initially by Barth *et al.*[35] and are commonly seen on fetal MRI, as well as secondary malformations due to prenatal hemorrhagic events. Brainstem malformations are a heterogeneous and complex group of pathologies[36], and neuroimaging, alongside genetic testing, plays a major role in detecting, classifying and describing these and other pathologies of the posterior fossa[37].

A limiting factor in biometric morphological fetal MRI studies is the small size of the structures of the posterior fossa. In the earliest examined fetus, at a gestational age of $14+0$ weeks, the cerebellar vermian area measured only 12.9 mm^2 and the brainstem was 68.2 mm^2. This makes imaging, especially in the early second trimester, prone to partial volume effects. Motion degradation is also limiting, but, in this study, all three subjects with motion artifacts were excluded. We did not use the same magnetic field-strength in all subjects (9.9% were acquired at 3-T), but the subgroup analysis showed no differences, in either diameter or area measurements, associated with the scanner type. We did not have a large population of fetuses without any pathological findings, so we relied on fetal MRI studies in cases with limb or body malformations and no known syndromes, which is common practice in fetal MRI studies. There was no systematic prenatal genetic testing, but all cases that had genetic abnormalities or syndromic features during postnatal follow-up were excluded. Furthermore, a subgroup analysis showed that there was no difference between subjects without and those with maternal and/or fetal pathological findings. There were only four cases < 18 gestational weeks, rendering the measurements more reliable from 18 weeks onwards.

In conclusion, we observed a differential spatiotemporal growth pattern of fetal brainstem substructures, characterized by an increase in area of the pons and decrease in that of the midbrain, relative to the total brainstem area, during the second and third trimesters of pregnancy *in vivo* and *in utero*. Our findings are in accordance with those of other biometric fetal MRI studies, although none of these focused on the relative contributions of these substructures. Caution is needed when interpreting fetal brainstem appearance during the early second trimester, as these brainstem proportions differ significantly from the adult morphology. With the provided reference data, fetal brainstem morphology can be quantified.

The reference data provided herein (Tables 1 and 2, Figures 2 and 4) may be used to increase the accuracy of the prenatal diagnosis of brainstem and cerebellar malformations.

REFERENCES

1. Haratz KK, Lerman-Sagie T. Prenatal diagnosis of brainstem anomalies. *Eur J Paediatr Neurol* 2018; **22**: 1016–1026.
2. Doherty D, Millen KJ, Barkovich AJ. Midbrain and hindbrain malformations: advances in clinical diagnosis, imaging, and genetics. *Lancet Neurol* 2013; **12**: 381–393.
3. Adamsbaum C, Moutard ML, Andre C, Merzoug V, Ferey S, Quere MP, Lewin F, Fallet-Bianco C. MRI of the fetal posterior fossa. *Pediatr Radiol* 2005; **35**: 124–140.
4. Atallah A, Guibaud L, Gaucherand P, Massardier J, des Portes V, Massoud M. Fetal and perinatal outcome associated with small cerebellar diameter based on second- or third-trimester ultrasonography. *Prenat Diagn* 2019; **39**: 536–543.
5. Snijders RJ, Nicolaides KH. Fetal biometry at 14–40 weeks' gestation. *Ultrasound Obstet Gynecol* 1994; **4**: 34–48.
6. Mirlesse V, Courtiol C, Althuser M, Cfef, Duyme M. Ultrasonography of the fetal brainstem: a biometric and anatomical, multioperator, cross-sectional study of 913 fetuses of 21-36 weeks of gestation. *Prenat Diagn* 2010; **30**: 739–745.
7. Ginath S, Lerman-Sagie T, Haratz Krajden K, Lev D, Cohen-Sacher B, Bar J, Malinger G. The fetal vermis, pons and brainstem: normal longitudinal development as shown by dedicated neurosonography. *J Matern Fetal Neonatal Med* 2013; **26**: 757–762.
8. Leibovitz Z, Shkolnik C, Haratz KK, Malinger G, Shapiro I, Lerman-Sagie T. Assessment of fetal midbrain and hindbrain in mid-sagittal cranial plane by three-dimensional multiplanar sonography. Part 1: comparison of new and established nomograms. *Ultrasound Obstet Gynecol* 2014; **44**: 575–580.
9. Leibovitz Z, Shkolnik C, Haratz KK, Malinger G, Shapiro I, Lerman-Sagie T. Assessment of fetal midbrain and hindbrain in mid-sagittal cranial plane by three-dimensional multiplanar sonography. Part 2: application of nomograms to fetuses with posterior fossa malformations. *Ultrasound Obstet Gynecol* 2014; **44**: 581–587.
10. Garel C, Chantrel E, Elmaleh M, Brisse H, Sebag G. Fetal MRI: normal gestational landmarks for cerebral biometry, gyration and myelination. *Childs Nerv Syst* 2003; **19**: 422–425.
11. Triulzi F, Parazzini C, Righini A. MRI of fetal and neonatal cerebellar development. *Semin Fetal Neonatal Med* 2005; **10**: 411–420.
12. Garel C. Fetal cerebral biometry: normal parenchymal findings and ventricular size. *Eur Radiol* 2005; **15**: 809–813.
13. Tilea B, Alberti C, Adamsbaum C, Armoogum P, Oury JF, Cabrol D, Sebag G, Kalifa G, Garel C. Cerebral biometry in fetal magnetic resonance imaging: new reference data. *Ultrasound Obstet Gynecol* 2009; **33**: 173–181.
14. Katorza E, Bertucci E, Perlman S, Taschini S, Ber R, Gilboa Y, Mazza V, Achiron R. Development of the Fetal Vermis: New Biometry Reference Data and Comparison of 3 Diagnostic Modalities-3D Ultrasound, 2D Ultrasound, and MR Imaging. *AJNR Am J Neuroradiol* 2016; **37**: 1359–1366.
15. Conte G, Milani S, Palumbo G, Talenti G, Boito S, Rustico M, Triulzi F, Righini A, Izzo G, Doneda C, Zolin A, Parazzini C. Prenatal Brain MR Imaging: Reference Linear Biometric Centiles between 20 and 24 Gestational Weeks. *AJNR Am J Neuroradiol* 2018; **39**: 963–967.
16. Ber R, Bar-Yosef O, Hoffmann C, Shashar D, Achiron R, Katorza E. Normal fetal posterior fossa in MR imaging: new biometric data and possible clinical significance. *AJNR Am J Neuroradiol* 2015; **36**: 795–802.
17. Vatansever D, Kyriakopoulou V, Allsop JM, Fox M, Chew A, Hajnal JV, Rutherford MA. Multidimensional analysis of fetal posterior fossa in health and disease. *Cerebellum* 2013; **12**: 632–644.
18. Prayer D, Malinger G, Brugger PC, Cassady C, De Catte L, De Keersmaecker B, Fernandes GL, Glanc P, Goncalves LF, Gruber GM, Laifer-Narin S, Lee W, Millischer AE, Molho M, Neelavalli J, Platt L, Pugash D, Ramaekers P, Salomon LJ, Sanz M, Timor-Tritsch IE, Tutschek B, Twickler D, Weber M, Ximenes R, Raine-Fenning N. ISUOG Practice Guidelines: performance of fetal magnetic resonance imaging. *Ultrasound Obstet Gynecol* 2017; **49**: 671–680.
19. Yushkevich PA, Piven J, Hazlett HC, Smith RG, Ho S, Gee JC, Gerig G. User-guided 3D active contour segmentation of anatomical structures: significantly improved efficiency and reliability. *Neuroimage* 2006; **31**: 1116–1128.
20. Borghi E, de Onis M, Garza C, Van den Broeck J, Frongillo EA, Grummer-Strawn L, Van Buuren S, Pan H, Molinari L, Martorell R, Onyango AW, Martines JC, WHO Multicentre Growth Reference Study Group. Construction of the World Health Organization child growth standards: selection of methods for attained growth curves. *Stat Med* 2006; **25**: 247–265.
21. Rigby RA, Stasinopoulos DM. Generalized additive models for location, scale and shape (with discussion). *Appl Statist* 2005; **54**: 507–554.
22. Cicchetti DV. Guidelines, criteria, and rules of thumb for evaluating normed and standardized assessment instruments in psychology. *Psychol Assess* 1994; **6**: 284–290.
23. Lumsden A, Krumlauf R. Patterning the vertebrate neuraxis. *Science* 1996; **274**: 1109–1115.
24. Sarnat HB. Disorders of segmentation of the neural tube: agenesis of selective neuromeres. In *Malformations of the Nervous System*. Elsevier: Amsterdam, 2007; 105–113.
25. Leto K, Arancillo M, Becker EB, Buffo A, Chiang C, Ding B, Dobyns WB, Dusart I, Haldipur P, Hatten ME, Hoshino M, Joyner AL, Kano M, Kilpatrick DL, Koibuchi N, Marino S, Martinez S, Millen KJ, Millner TO, Miyata T, Parmigiani E, Schilling K, Sekerkova G, Sillitoe RV, Sotelo C, Uesaka N, Wefers A, Wingate RJ, Hawkes R. Consensus Paper: Cerebellar Development. *Cerebellum* 2016; **15**: 789–828.
26. Garda A-L, Echevarría D, Martínez S. Neuroepithelial co-expression of Gbx2 and Otx2 precedes Fgf8 expression in the isthmic organizer. *Mech Dev* 2001; **101**: 111–118.

27. Landsberg RL, Awatramani RB, Hunter NL, Farago AF, DiPietrantonio HJ, Rodriguez CI, Dymecki SM. Hindbrain rhombic lip is comprised of discrete progenitor cell populations allocated by Pax6. *Neuron* 2005; **48**: 933–947.
28. Wingate RJT. The rhombic lip and early cerebellar development. *Curr Opin Neurobiol* 2001; **11**: 82–88.
29. Doherty D, Millen KJ, Barkovich AJ. Midbrain and hindbrain malformations: advances in clinical diagnosis, imaging, and genetics. *Lancet Neurol* 2013; **12**: 381–393.
30. Caughey AB, Hopkins LM, Norton ME. Chorionic Villus Sampling Compared With Amniocentesis and the Difference in the Rate of Pregnancy Loss. *Obstet Gynecol* 2006; **108**: 612–616.
31. Devisme L, Bouchet C, Gonzales M, Alanio E, Bazin A, Bessieres B, Bigi N, Blanchet P, Bonneau D, Bonnieres M, Bucourt M, Carles D, Clarisse B, Delahaye S, Fallet-Bianco C, Figarella-Branger D, Gaillard D, Gasser B, Delezoide AL, Guimiot F, Joubert M, Laurent N, Laquerriere A, Liprandi A, Loget P, Marcorelles P, Martinovic J, Menez F, Patrier S, Pelluard F, Perez MJ, Rouleau C, Triau S, Attie-Bitach T, Vuillaumier-Barrot S, Seta N, Encha-Razavi F. Cobblestone lissencephaly: neuropathological subtypes and correlations with genes of dystroglycanopathies. *Brain* 2012; **135**: 469–482.
32. Glickstein M, Doron K. Cerebellum: connections and functions. *Cerebellum* 2008; **7**: 589–594.
33. Perrini P, Tiezzi G, Castagna M, Vannozzi R. Three-dimensional microsurgical anatomy of cerebellar peduncles. *Neurosurg Rev* 2013; **36**: 215–224; discussion 224–225.
34. Hatta T, Satow F, Hatta J, Hashimoto R, Udagawa J, Matsumoto A, Otani H. Development of the pons in human fetuses. *Congenit Anom (Kyoto)* 2007; **47**: 63–67.
35. Barth PG. Pontocerebellar hypoplasias. An overview of a group of inherited neurodegenerative disorders with fetal onset. *Brain Dev* 1993; **15**: 411–422.
36. Barkovich AJ, Millen KJ, Dobyns WB. A developmental classification of malformations of the brainstem. *Ann Neurol* 2007; **62**: 625–639.
37. Massoud M, Guibaud L. Prenatal imaging of posterior fossa disorders. *A review. Eur J Paediatr Neurol* 2018; **22**: 972–988.

SUPPORTING INFORMATION ON THE INTERNET

The following supporting information may be found in the online version of this article:

Table S1 Maternal and fetal pathological findings indicating fetal brain magnetic resonance imaging in the study group

Table S2 Numbers of fetuses measured at each gestational week (GW). The gestational age ranged from 14 + 0 (GW = 15) to 39 + 2 (GW = 40) weeks. There are three peaks at which fetal MRI is commonly performed: GW 21, 24 and 28